Title	Effect of spray impingement distance on piston top fuel adhesion in direct injection gasoline engines
Author(s)	Luo, Hongliang; Nishida, Keiya; Uchitomi, Shintaro; Ogata, Youichi; Zhang, Wu; Fujikawa, Tatsuya
Citation	International Journal of Engine Research , 21 (5) : 742 - 754
Issue Date	2020-06-01
DOI	10.1177/1468087418774175
Self DOI	
URL	https://ir.lib.hiroshima-u.ac.jp/00051076
Right	Luo H, Nishida K, Uchitomi S, Ogata Y, Zhang W, Fujikawa T. Effect of spray impingement distance on piston top fuel adhesion in direct injection gasoline engines. International Journal of Engine Research. 21(5), pp.742-754. Copyright © 2020 Authors. doi:10.1177/1468087418774175 This is not the published version. Please cite only the published version. この論文は出版社版ではありません。引用の際には出版社版をご確認、ご利用ください。
Relation	

Effect of Spray Impingement Distance on Piston Top Fuel Adhesion in Direct Injection Gasoline Engines

---

Hongliang LUO[1*], Keiya NISHIDA[1], Shintaro UCHITOMI[1], Youichi OGATA[1], Wu ZHANG[2], Tatsuya FUJIKAWA[2]

[1]Department of Mechanical System Engineering, Hiroshima University, 1-4-1 Kagamiyama, Higashi-Hiroshima 739-8527, Japan.

[2]Mazda Motor Corporation, 3-1 Shinchi, Fuchu-cho, Aki-gun, Hiroshima 730-8670, Japan

Abstract

Direct injection is an attractive technology for improving fuel economy and engine performance in gasoline engines. However, the adhered fuel formed on the piston surface has significant influence on the combustion efficiency and emissions. To obtain a better understanding of fuel adhesion, this work involved investigation of the spray and impingement on a flat wall through a mini-sac injector with a single hole. Different impingement distances and injection pressures were investigated. The evolution of the impinging spray was obtained by the Mie scattering method. The refractive index matching method was applied to measure fuel adhesion. The mass, area, and thickness of adhesion under different conditions were compared. The experimental results show that the fuel adheison on the wall increases significantly with a large impingement distance. Moreover, the maximum thickness increases and the thickness uniformity of the fuel adhesion declines under a large impingement distance condition.

Keywords

1 INTRODUCTION

Direct injection (DI) is a promising technology to achieve the requirements of low-pollutant emission and high-energy efficiency imposed by increasingly stringent regulations on engine emissions. This is owing to the better air and mixture control by direct injection compared to port fuel injection[1-3]. However, the impingement of liquid fuel on the wall of the combustion chamber and piston is a major drawback of this technique, because wall wetting leads to pool fires linked with rich diffusion flames on the top of the liquid deposit [4,5]. This can contribute to unwanted pollutant formation and an increase in unburned hydrocarbons [6–8]. As governmental regulations demand a low threshold of emissions on gasoline engine, it has become increasingly important for car manufacturers to minimize these effects [9,10].

As a result, there are numerous reports regarding fuel adhesion on the wall. The optical technique of the refractive index matching (RIM) method was developed by Drake et al. [11–13] to investigate fuel adhesion mass, area, and thickness with millisecond temporal and spatial resolutions. Then, Yang and Ghandhi [14] used the RIM method to show that the ambient pressure had a strong effect on fuel adhesion. Maligne and Bruneaux [15] observed "discrete pockets" and "continuous film" structures on the wall after impingement. Zheng et al. [16] compared the fuel adhesion results by the RIM method and CFD simulation, and noted a significant effect of the ambient temperature on the thickness. Otachi et al. [17] studied the pressure effects on fuel spray impinging on the wall. Other methods were also applied to investigate the fuel adhesion on the wall. Fujimoto et al. [18–21] investigated the fuel spray impinging on the flat wall under both gasoline and diesel engine conditions. Akop et al. [22–25] weighed the adhered fuel mass on an impingement disk wall and characterized the fuel adhesion under different conditions. Both Cheng et al. [26] and Schulz et al. [27,28] conducted experimental studies on fuel adhesion using the laser-induced fluorescence (LIF) technique. Yu et al. [29,30] evaluated the impingement characteristic and weighed the fuel adhesion to investigate the impingement process.

As reviewed above, there is a considerable number of investigations on fuel adhesion, whereas research on the three views of the impinging spray process has seldom been reported. Moreover, the effect of pressure and wall roughness on the adhered fuel formation has been reported in our previous papers [31,32]. In the present work, the effect of impingement distance on fuel adhesion was discussed based on the three views of impinging spray. Experiments were performed in a constant high-pressure chamber. The impinging spray developments were compared under different injection pressures and impingement distances. The front view and side view were obtained by Mie scattering, and the radius of impinging spray (R_s), vortex height of impinging spray (H_v), spray tip penetration (S), and impinging spray height (H_i) were also studied. The bottom view was acquired by the RIM method, and the mass, area, and thickness of the fuel adhesion were investigated. Specifically, all the results were time-resolved to better understand the impinging spray of a gasoline engine.

2. EXPERIMENTAL DETAILS

2.1 Experimental apparatus

The experimental apparatus of the Mie scattering for spray image observation in the current study is shown in Figure 1, where 1(a) is the front view of the spray apparatus, and 1(b) is the side view. The apparatus consisted of a constant high-pressure chamber, injection system, and optical system. Toluene was injected into a mini-sac injector by a high-pressure injection system. A high-speed video camera (Photron FASTCAM SAZ) set at 40,000 frames per second (fps) with a resolution of 1024 × 512 pixels was utilized for spray observation. A xenon lamp (Ushio SX-131 UID501XAMQ) placed at a position perpendicular to the camera was applied to illuminate the spray. The injector and camera were synchronized by a delay generator. Different windows of the chamber were used for different views.

The experimental apparatus of RIM measurement for fuel adhesion is shown in Figure 2. The constant high-pressure chamber and injection system were the same as those in the Mie

scattering experiment, but the optical system was different. A reflection mirror was placed

directly beneath the impingement plate. A xenon lamp was positioned at the side window to

emit continuous and high-intensity light with an incident angle of approximately 5°. A high-

speed video camera with a frame rate of 10,000 fps and a resolution of 512 × 512 pixels was

used to capture the fuel adhesion images through the mirror.

2.2 Experimental conditions

The reduction of particulate number (PN) emissions is the major concern of a gasoline DI

engine due to the introduction of PN standards in Euro 6 emission regulations. During the

catalyst-warm-up operation, the retarded injection timing is used to increase the exhaust gas

temperature. Although multiple-injection strategy is used to reduce the wall wetting, the late

injection near top dead center (TDC) resulted in an increase in PN emissions. To clarify the

spray-wall interactions under the aforementioned engine conditions, the equivalent

experimental conditions in the constant volume chamber were determined in Table 1. The

fuel tested in this study was toluene, as a surrogate fuel for gasoline. The injection mass was

kept constant at 3.0 mg equivalent to the total injection quantity of the multi-hole injector

divided by hole number. The injection pressures changed from 10 to 30 MPa considering the

phenomena, resulting in different injection durations of 2.4, 1.65, and 1.35 ms. The ambient

density of non-evaporating conditions is kept the same as that of in-cylinder conditions. A

mini-sac injector with a single hole (0.135 mm) was used. To determine the effect of

impingement distance on fuel adhesion, it ranged between 28 and 40 mm from the nozzle exit

to the wall along the spray axis. The impingement angle was 45° from the spray axis to the flat

wall. The surface roughness of the new piston used in gasoline engine is approximately Ra1.0, but

it may increase up to Ra10.0 or more due to deposit accumulation[31]. Therefore, a circle plate

made of quartz glass with surface roughness of Ra7.5 was placed under the injector as a flat

wall, representing a used piston in the engine. As shown in Figure 3, the diameter of the plate

1   was 50 mm and its thickness was 2 mm. The coordinate system was defined, and the

2   intersection point o of the spray axis and the wall was defined as the impingement point.

3   **2.3 Image processing**

4   The parameters such as radius of impinging spray (R_s), vortex height of impinging spray

5   (H_v), spray tip penetration (S), and impinging spray height (H_i) are widely used to perform

6   spray–wall impingement analyses [29,33,34]. These values were experimentally obtained from

7   raw images by determining the edge of the impinging spray using inhouse code created by

8   ourselves in the MATLAB software.

9   The dotted line in Figure 4 represents the wall surface. The focus of the front and side

10   views is on the impingement point plane and spray axis plane, respectively. R_s and H_v are

11   defined from the front view. R_s is the maximum horizontal distance from the spray center to

12   the furthest edge of the spray. H_v is the maximum distance from the wall surface to the edge of

13   the spray vortex. S and H_i are defined from the side view. Generally, the spray tip penetration

14   is defined as the distance from the nozzle hole exit to the spray tip. However, after the wall

15   impingement, the penetration is not only the distance from the nozzle hole to the

16   impingement point, but also the radial distance from the impingement point to the furthest

17   location of the fuel [31,35]. Therefore, S is defined as the sum of impinging distance (D_{imp}) and

18   radial distance (D_{rad}). H_i is the maximum vertical distance from the wall surface to the edge of

19   the impinging spray. Results of the front and side views were obtained from a clear spray by

20   binarizing the images. The fuel adhesion data were obtained from the bottom view. All the

21   results were calculated three times under each specific set of experimental conditions, and the

22   average values were presented.

1   The spatial distribution of the fuel adhesion was measured by the RIM technique. Drake et

2   al. [12] showed the relationship between the adhesion thickness $h(x, y)$ and the intensity

3   reduction of the scattered light $\Delta I(x, y)$ as follows:

4

$$\Delta I(x, y) = 1 - \frac{I_{wet}(x, y)}{I_{ref}(x, y)} \qquad (1)$$

5   where $I_{ref}(x, y)$ is the scattered light intensity of the dry image at the location *(x, y)*, and

6    $I_{wet}(x, y)$ is the light intensity of adhered fuel on the wall at *(x, y)*.

7   After the calibration procedure, a correlation of $h(x, y)$ and $\Delta I(x, y)$ can be formulated:

8

$$h(x, y) = f(\Delta I) \qquad (2)$$

9   To obtain the calibration curves, a calibration experiment was carried out under

10   atmospheric conditions without the injection system. Two different fuels were selected

11   because tridecane has low volatility and high viscidity, but toluene has high volatility and low

12   viscidity. Moreover, their refractive index is similar to that of the quartz glass. A much thinner

13   thickness of fuel adhesion can be obtained with a liquid mixture of these fuels. The

14   characteristics of the fuels and quartz glass are summarized in Table 2.

15   A mixture (10% volume of tridecane and 90% volume of toluene) was used for the

16   calibration procedure. The fuel mixture was dripped on the dry window by means of a syringe

17   and the reduction in scattering light increased from 0 to the maximum value. After a certain

18   volume of the mixture was dripped on the rough quartz, the droplet rapidly expanded, and the

19   area of fuel increased rapidly. During this time, toluene, which is the high volatility component,

20   quickly evaporated; however, there was only a slight increase in the scattered light. Once the

21   adhesion area reached a certain value, tridecane, which is the low volatility component,

22   begins to evaporate, and the scattered light changed significantly. There are two hypotheses in

23   this case: one stating that all the toluene has evaporated, but all the tridecane has not yet

evaporated; another stating that the thickness of fuel adhesion is uniform. Thus, $h(x, y)$ can be calculated because the tridecane volume was calculated as 10% of the mixture, and the averaged reference dry image was obtained before the liquid deposited on the glass. Then $\Delta I(x, y)$ can be calculated using Equation (1). Eventually, one point with $h(x, y)$ and $\Delta I(x, y)$ was obtained. By varying the mixture volume from 0.1 μL to 10 μL, the calibration curve was acquired by Equation (2). The calibration curves for 28 mm and 40 mm are plotted in Fig. 5. The horizontal axis is the reduction in scattered light, and the vertical axis is fuel adhesion thickness. It shows that fuel adhesion thickness at a certain reduction in scattered light for 40 mm is larger than that for 28 mm.

After the calibration calculation, the fuel adhesion thickness can be measured through the RIM method. The image processing of the RIM experiment is shown in Figure 6. First, a dry image was acquired. Then, it was subtracted by the wet image to obtain only the adhered fuel image, and the $\Delta I(x, y)$ can be obtained by this image. Finally, the thickness distribution was calculated through the calibration curve. The adhered fuel area and mass can also be integrated from the pixels of each thickness. Additional details about RIM method can be found in our previous studies [31,32].

3. RESULTS AND DISCUSSION

3.1 Characteristics of impinging spray

Figure 7 shows R_s under three conditions (P_{inj} = 10, 20, and 30 MPa). The horizontal axis is the time after start of injection, and R_s is in the vertical axis. R_s of D_{imp} = 28 mm is larger than that of D_{imp} = 40 mm under all conditions. The ambient pressure (P_{amb} = 0.5 MPa) results in strong interaction between the fuel and nitrogen, decelerating the droplets before impingement. During the spray propagation at the shorter impingement distance, the fuel with higher Weber number diffuses around after impingement on the wall. As a result, R_s of

D_{imp} = 28 mm is larger than that of D_{imp} = 40 mm. Moreover, R_s increases with an increase in the injection pressure. It can be expected that the increased injection pressure enhances the kinetic energy of fuel.

Figure 8 shows H_v under three conditions (P_{inj} = 10, 20, and 30 MPa). The horizontal axis is the time after start of injection, and H_v is in the vertical axis. H_v of D_{imp} = 28 mm is larger than that of D_{imp} = 40 mm under all conditions. Owing to its shorter impingement distance, the fuel with higher Weber number and momentum impinges on the wall, leading to a decreasing number of droplets depositing on the wall, and an increasing number of splashing droplets [36]. Therefore, H_v of D_{imp} = 28 mm is larger than that of D_{imp} = 40 mm. In contrast to the different injection pressures, H_v increases more rapidly with an increase in injection pressure. It can be expected that the increased injection pressure enhances the Weber number and the initial kinetic energy of the fuel spray, resulting in faster vortex generation.

Figure 9 presents $S,$ and the impingement distance is shown by the broken line. Three conditions (P_{inj} = 10, 20, and 30 MPa) were investigated. For all conditions, the spray development can be divided into two stages. It increases almost linearly before impingement, and the gradient of S decreases after spray impingement [31]. The drag force from the wall and ambient gas can be regarded as the main reasons for this phenomenon. It is noteworthy that before impingement, S is almost the same under different impingement distances. However, after impingement, S of D_{imp} = 40 mm is slightly larger than that of D_{imp} = 28 mm under all conditions. One possible reason is that, after impingement, the fuel disperses and spreads in all directions, with the result that the interaction between the droplets and air is much stronger than before. Moreover, friction from the wall can be regarded as another reason. As a result, S increases with the increased impingement distance. Additionally, under different injection pressures, the S of 30 MPa is larger than that of 10 MPa, and the impingement time of 30 MPa is shorter than that of 10 MPa owing to higher Weber number of the spray.

1 Figure 10 presents H_i under three conditions (P_{inj} = 10, 20, and 30 MPa). The horizontal

2 axis is the time after start of injection, and H_i is in the vertical axis. It is clear that H_i of D_{imp} =

3 28 mm is larger than that of D_{imp} = 40 mm under all conditions. This phenomenon can be

4 attributed to the different momentum of the droplets impinging on the wall. The droplets of

5 D_{imp} = 28 mm have higher Weber number when impinging on the wall, and many droplets

6 splash around after impingement, resulting in larger H_i compared with that of D_{imp} = 40 mm.

7 In contrast to different conditions, H_i increases and the gradient of H_i becomes larger owing to

8 the effect of the enhanced kinetic energy of fuel.

9 **3.2 Characteristics of fuel adhesion**

10 During the spray, some scattered light from the floating droplets above the impingement

11 region. In order to eliminate the stray light error, all results are after the end of injection

12 (EOI)[31].

13 Figure 11 shows the evolution of the adhered fuel under different conditions. The fuel

14 adhesions on the wall at 5, 10, 20, and 40 ms ASOI are shown. The pseudocolor represents the

15 adhered fuel thickness, varying from 0 to 2.5 μm, and the impingement point is shown by the

16 cross symbol. Under each condition, all cases at different times show similar structures, and

17 the fuel adhesion areas are almost symmetric. It is evident that the wetted area increases

18 under higher injection pressure, and the better atomization of a high injection pressure

19 should be responsible for this. More importantly, when D_{imp} = 28 mm, the fuel adhesion

20 becomes a little thicker at the upstream, whereas when D_{imp} = 40 mm, the thicker region

21 moves downstream. There may be two reasons for this. One is that there are different impact

22 regimes for droplets impinging on the wall: "stick," "spread," and "splash" [32]. The increased

23 impingement distance decelerates the droplets owing to the ambient pressure (P_{amb} = 0.5

24 MPa). Thus, after impingement on the wall, some droplets may change their behavior from

25 "splash" to "spread," or even to "stick", resulting in thicker fuel adhesion of D_{imp} = 40 mm. The

second reason may be that even though some droplets splash off the wall, the droplets with low velocity easily drop back on the wall, causing the thicker fuel adhesion to move down.

The fuel adhesion mass and area are depicted in Figures 12 and 13. The adhesion mass ratio is defined as the ratio of adhesion mass to total injection mass. The fuel adhesion mass and area increase with time even after the end of injection because there are still some droplets dropping on the wall. An increase in injection pressure under a certain ambient pressure increases the fuel adhesion mass and area owing to better atomization. Furthermore, both fuel adhesion mass and area increase at a large impingement distance. A decrease in the number of splashing droplets tends to be responsible, which agrees well with the Mie scattering results. Additionally, the bigger spray width and better atomization should be other reasons for this. Park et al. [37] have already proven that the spray width increases as the spray flows downstream, and the SMD decreases at a large impingement distance. Therefore, the wider spray and better atomization of D_{imp} = 40 mm is formed before impingement, resulting in bigger adhesion area and mass on the wall. The same tendency of the wider fuel adhesion at D_{imp} = 40 mm, can also be observed in the comparison between Figures 11 (b) and (c).

Figure 14 shows the adhesion mass ratio under different conditions at 40 ms ASOI. For D_{imp} = 28 mm, the adhesion mass ratio increases from 2.9% to 3.7% with an increase in injection pressure. However, by increasing the D_{imp} to 40 mm, the ratio increases from 7.8% to 8.6% at increased injection pressures, and thus, the ratios of D_{imp} = 40 mm are more than twice at D_{imp} = 28 mm.

To further investigate the adhesion thickness, the probability of thickness was determined. As shown in Figure 15, the horizontal axis is the fuel adhesion thickness, and the vertical axis is the probability of mass. The probability of mass is based on the value of each pixel, and the probability must satisfy the normalization conditions:

$$\sum_{i=0}^{\infty} f_M\left(h_i\right) = 1 \qquad (3)$$

where the sum of fuel adhesion mass in the thickness fraction between $h - \Delta h$ and h is defined as $M(h)$, $f_M(h)$ is the probability of $M(h)$, and Δh is 0.05 μm.

Figure 15 describes the probability of thickness with different times at P_{inj} = 30 MPa and D_{imp} = 28 mm, and the average values of three shots were presented. It is reported that the peak value of the curves decreases, and the curve becomes a little wider with time, which indicates that the uniformity of adhesion thickness becomes worse with time. And the same observation can be derived from Figure 11 (b). One possible explanation could be that some rebounding and splashing droplets fall on the wall.

Figure 16 illustrates the effects of impingement distance and injection pressure on adhesion thickness, and the average values of three shots were presented. First, the results of D_{imp} = 28 mm are examined. Only one peak value exists and the increased injection pressure causes the curve to shift to the left, leading to thinner fuel adhesion. It can be argued that high injection pressure improves the atomization and dispersion of droplets, resulting in thinner fuel adhesion, and the same conclusion can be drawn from the comparison between Figures 11 (a) and (b). Secondly, there are two peak values with D_{imp} = 40 mm, which indicates that an increase in impingement distance deteriorates the uniformity of adhesion thickness. The transition of "splash" to "spread" and "stick" phenomenon could be a possible explanation for this. The same observation can also be noted from the comparison of Figures 11 (b) and (c). It is interesting to find that the maximum thickness with D_{imp} = 40 mm is approximately 2.2 μm, and it is larger than that with D_{imp} = 28 mm. The main possible reason is that the number of splashing droplets decreases owing to low velocity at a large impingement distance.

Further investigation was carried out to clarify the effect of impingement distances on the distribution of fuel adhesion thickness (shown in Figure 17). The fuel adhesion was divided by

y = 0, 10, and 20mm lines that represent the upstream, midstream, and downstream of the fuel adhesion. When D_{imp} = 28 mm, the fuel adhesion thickness decreases from upstream to downstream, and the uniformity of thickness improves from upstream to downstream. However, when D_{imp} = 40 mm, the fuel adhesion thickness increases from upstream to midstream, and then decreases from midstream to downstream. The changed regime of the droplets, from "splash" to "spread" with a large impingement distance is a possible explanation for that distribution pattern. Furthermore, when D_{imp} = 40 mm, the thickness uniformity on upstream is similar to that occurring on midstream, but both uniformities are worse than that located on downstream. In contrast to other impingement distances, the fuel adhesion on upstream and midstream becomes thicker with a large impingement distance, and the uniformity of thickness deteriorates with a large impingement distance. On the contrary, the fuel adhesion on downstream shows a slight change.

4. CONCLUSIONS

The characteristics of fuel spray and adhesion under different impingement distances and injection pressures were investigated experimentally. The values of R_s, H_v, S, and H_i were acquired, and the fuel adhesion evolution was analyzed. Furthermore, the probabilities of adhesion thickness and thickness distribution were discussed. The major conclusions are as follows:

1. With a large impingement distance under ambient condition, the velocity of droplets decreases significantly, resulting in more droplets adhering to the wall instead of splashing out of the wall. As a result, R_s, H_v, and H_i decrease with an increase in impingement distance. However, after impingement, owing to the stronger drag force by the ambient gas and friction from the wall, S increases with the increase in impingement distance.

12

2. Both the high injection pressure and large impingement distance increase the fuel adhesion mass and area, but the mechanisms are different. Owing to better atomization with high injection pressure, the fuel adhesion on the wall increases. At a large impingement distance, the lower velocity, bigger spray width, and better atomization are the main reasons for increased fuel adhesion on the wall after impingement.

3. Under the large impingement distance condition, more fuel adheres on midstream and the thickness uniformity of fuel adhesion becomes worse. Moreover, the maximum thickness of fuel adhesion increases with a large impingement distance.

It should be noticed that although the high injection pressure favors better atomization of fuel, the fuel adhesion on the piston head may increase under catalyst-warm-up condition, which has to be handled with care. More importantly, with long impingement distance, the fuel adhesion mass and area increase significantly under catalyst-warm-up condition, leading to the pool flame to originate more soot emission, which should be considered in the design of direct injection gasoline engines. Further investigation on adhered fuel formation and spray behavior should be undertaken, and the evaporation condition should be considered in future work.

REFERENCES

1. Li K, Nishida K, Ogata Y, et al. Effect of flat–wall impingement on diesel spray combustion. *Proceedings of the Institution of Mechanical Engineers, Part D: Journal of Automobile Engineering* 2015; 229(5): 535-549.

2. Lacey J, Kameshwaran K, Sathasivam S, et al. Effects of refinery stream gasoline property variation on the auto-ignition quality of a fuel and homogeneous charge compression ignition combustion. *International Journal of Engine Research* 2017; 18(3): 226-239.

3. Nishida K, Zhu J, Leng X, et al. Effects of micro-hole nozzle and ultra-high injection pressure on air entrainment, liquid penetration, flame lift-off and soot formation of diesel spray flame. *International Journal of Engine Research* 2017; 18(1-2): 51-65.

4. Montanaro A, Malaguti S, and Alfuso S. Wall impingement process of a multi-hole GDI spray: Experimental and numerical investigation. SAE Technical Paper 2012-01-1266, 2012.

5. Yao M, Zheng Z, and Liu H. Progress and recent trends in homogeneous charge compression ignition (HCCI) engines. *Progress in Energy and Combustion Science* 2009; 35(5): 398-437.

6. Kiplimo R, Tomita E, Kawahara N, et al. Effects of spray impingement, injection parameters, and EGR on the combustion and emission characteristics of a PCCI diesel engine. *Applied Thermal Engineering* 2012; 37: 165-175.

7. Liu H, Zhong Z, Zheng Z, et al. Study of the control strategies on soot reduction under early-injection conditions on a diesel engine. *Fuel* 2015; 139:472-81.

8. Henkel S, Beyrau F, Hardalupas Y, et al. Novel method for the measurement of liquid film thickness during fuel spray impingement on surfaces. *Optics express* 2016; 24(3): 2542-2561.

9. Maricq MM. Chemical characterization of particulate emissions from diesel engines: *A review. Journal of Aerosol Science* 2007; 38(11): 1079-1118.

10. Berggren C and Magnusson T. Reducing automotive emissions—The potentials of combustion engine technologies and the power of policy. *Energy Policy* 2012; 41: 636-643.

11. Drake MC, Fansler TD, and Rosalik ME. Quantitative high-speed imaging of piston fuel films in direct-injection engines using a refractive-index-matching technique. In: *The 15th Annual Conference on Liquid Atomization and Spray Systems*, Madison, WI, 15-17 May 2002,1-8.

12. Drake MC, Fansler TD, Solomon AS, et al. Piston fuel films as a source of smoke and hydrocarbon emissions from a wall-controlled spark-ignited direct-injection engine. SAE Technical Paper 2003-01-0547, 2003.

13. Drake MC and Haworth DC. Advanced gasoline engine development using optical diagnostics and numerical modeling. *Proceedings of the Combustion Institute* 2007; 31(1): 99-124.

14. Yang B and Ghandhi J. Measurement of diesel spray impingement and fuel film characteristics using refractive index matching method. SAE Technical Paper 2007-01-0485, 2007.

15. Maligne D and Bruneaux G. Time-resolved fuel film thickness measurement for direct injection SI engines using refractive index matching. SAE Technical Paper 2011-01-1215, 2011.

16. Zheng Y, Xie X, Lai MC, et al. Measurement and simulation of DI spray impingements and film tics. In: *The 12th Triennial Int. Conf. on Liquid Atomization and Spray Systems*, Heidelberg, Germany, 2–6 Sep. 2012, 1-8.

17. Otachi T, Paku K, Nishida K, et al. Characteristics of flat-wall-impinging fuel spray: vapor phase distribution and liquid film adhesion. In: *The 13th Triennial Int. Conf. on Liquid Atomization and Spray Systems*, Tainan, Taiwan, 23–27 Aug 2015, 1-8.

18. Fujimoto H, Sato GT, Kuniyoshi H, et al. Investigation of combustion in medium-speed marine diesel engines using model chambers. *Conseil International des Machines a Combustion* 1977; B:1853-1861.

19. Katsura N, Saito M, Senda J, et al. Characteristics of a diesel spray impinging on a flat wall. SAE Technical Paper 890264, 1989.

20. Fujimoto H, Senda J, Nagae M, et al. Characteristics of a diesel spray impinging on a flat wall. *In International Symposium COMODIA* 1990; 90: 193-198.

21. Senda J, Ohnishi M, Takahashi T, et al. Measurement and Modeling on Wall Wetted Film Profile and Mixture Preparation in Intake Port of SI Engine. SAE Technical Paper 1999-01-0798, 1999.

22. Akop MZ, Zama Y, Furuhata T, et al. Experimental investigations on adhered fuel and impinging diesel spray normal to a wall. *Atomization and Sprays* 2013; 23(3): 211–231.

23. Akop MZ, Zama Y, Furuhata T, et al. Characteristics of adhesion diesel fuel on an impingement disk wall. Part 1: Effect ofimpingement area and inclination angle of disk. *Atomization and Sprays* 2013; 23(8): 725–744.

24. Akop MZ, Zama Y, Furuhata T, et al. Characteristics of adhesion diesel fuel on an impingement disk wall. Part 3: Ambient pressure effect. *Atomization and Sprays* 2014; 24(7): 625-650.

25. Akop MZ, Zama Y, Furuhata T, et al. Characteristics of adhesion diesel fuel on an impingement disk wall. Part 2: Droplet Weber number and adhered fuel mass. *Atomization and Sprays* 2014; 24(8): 651-671.

26. Cheng YS, Deng K, and Li T. Measurement and simulation of wall-wetted fuel film thickness. *Int. J. Thermal Sci.* 2010; 49(4): 733–739.

27. Schulz F, Schmidt J, Beyrau F. Development of a sensitive experimental set-up for LIF fuel wall film measurements in a pressure vessel. *Experiments in Fluids* 2015; 56(5): 1-16.

28. Schulz F, Samenfink W, Schmidt J, et al. Systematic LIF fuel wall film investigation. *Fuel* 2016; 172: 284–292.

29. Yu H, Liang X, Shu G, et al. Experimental investigation on spray-wall impingement characteristics of n-butanol/diesel blended fuels. *Fuel* 2016; 182: 248-258.

30. Yu H, Liang X, Shu G, et al. Experimental investigation on wall film ratio of diesel, butanol/diesel, DME/diesel and gasoline/diesel blended fuels during the spray wall impingement process. *Fuel Processing Technology* 2017; 156: 9-18.

31. Luo H, Shintaro U, Nishida K, et al. Experimental Investigation on Fuel Film Formation of Spray Impingement on Flat Walls with Different Surface Roughness. *Atomization and Sprays* 2017; 27(7): 611–628.

32. Luo H, Shintaro U, Nishida K, et al. Fuel Adhesion Characteristics of Flat Wall-Impinging Spray under DISI Engine Conditions. In: *The 29th Annual Conference on Liquid Atomization and Spray Systems-Americas*, Atlanta, GA, 15-18 May 2017, 1-13.

33. Park SW, Lee CS. Macroscopic and microscopic characteristics of a fuel spray impinged on the wall. *Experiments in fluids* 2004; 37(5): 745-762.

34. Andreassi L, Ubertini S, Allocca L. Experimental and numerical analysis of high pressure diesel spray–wall interaction. *International journal of multiphase flow* 2007; 33(7): 742-765.

35. Guo M, Kishi R, Shi B, et al. Effects of cross-flow on fuel spray injected by hole-type injector for direct injection gasoline engine. *Atomization and Sprays* 2015; 25(1): 81-98.

36. Bai C, Gosman AD. Development of methodology for spray impingement simulation. SAE Technical Paper 950283, 1995.

37. Park SW, Lee CS. Macroscopic and microscopic characteristics of a fuel spray impinged on the wall. *Experiments in fluids* 2004; 37(5): 745-762.

1   **APPENDIX**

2   **Notation**

3   *ASOI   After Start of Injection*

4   *d   Nozzle Hole Diameter (mm)*

5   *Dimp   Impingement Distance (mm)*

6   *D_{rad} Radical Distance after Impingement (mm)*

7   *DI   Direct Injection*

8   *EOI   End of Injection*

9   *fps   Frames Per Second*

10   *H_i Impinging Spray Height (mm)*

11   *H_v Vortex Height of Impinging Spray (mm)*

12   *LIF   Laser-Induced Fluorescence*

13   *M_{inj} Injection Mass (mg)*

14   *P_{inj} Injection Pressure (MPa)*

15   *P_{amb} Ambient Pressure (MPa)*

16   *PN   Particulate Number*

17   *Ra   Arithmetical Mean Deviation of the Profile (μm)*

18   *RIM   Refractive Index Matching*

19   *R_s Radius of Impinging Spray (mm)*

20   *S   Spray Tip Penetration (mm)*

21   *t_d Injection Duration (ms)*

22   *TDC   Top Dead Center*

23   *T_{amb} Ambient Temperature (K)*

24   *ρ_{amb} Ambient Density (kg/m^3)*

1   θ_{imp} *Impingement Angle (deg)*

2   *h*   *Fuel Adhesion Thickness* (μm)

3   *x*   *Location at x Direction Coordinate Value (mm)*

4   *y*   *Location at y Direction Coordinate Value (mm)*

5   ΔI *Intensity Reduction of Scattered Light*

6   I_{ref} *Scattered Light Intensity of Dry Image*

7   I_{wet} *Scattered Light Intensity of Wet Image*

8     $M(h)$ *Sum of Fuel Adhesion Mass (mg)*

9     $f_M(h)$ *Probability of Fuel Adhesion Mass (%)*

Figures:

(a) Front view   (b) Side view
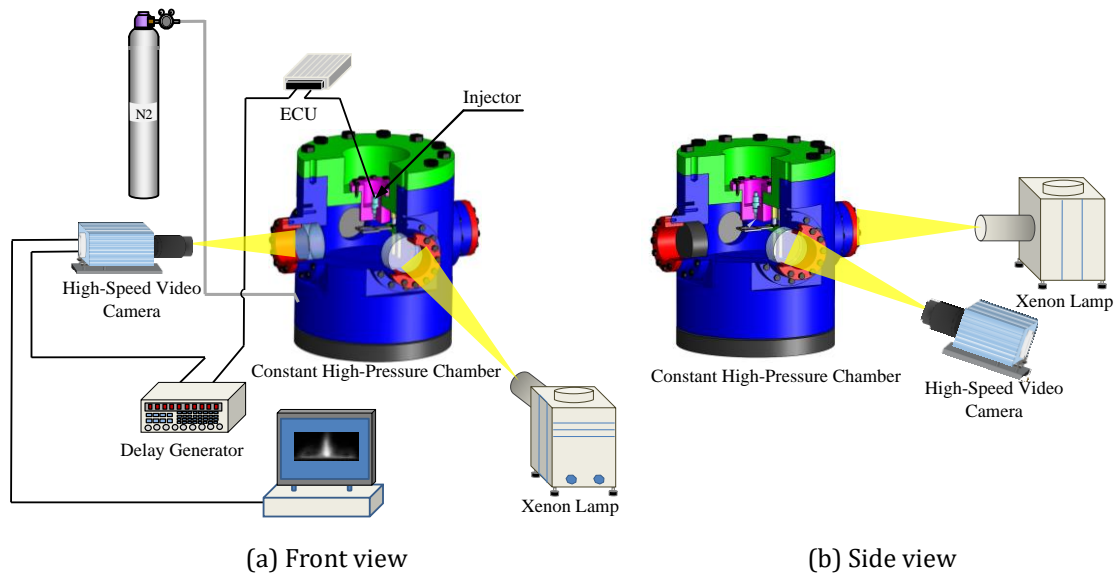
Figure 1. Experimental apparatus of Mie scattering for spray image observation
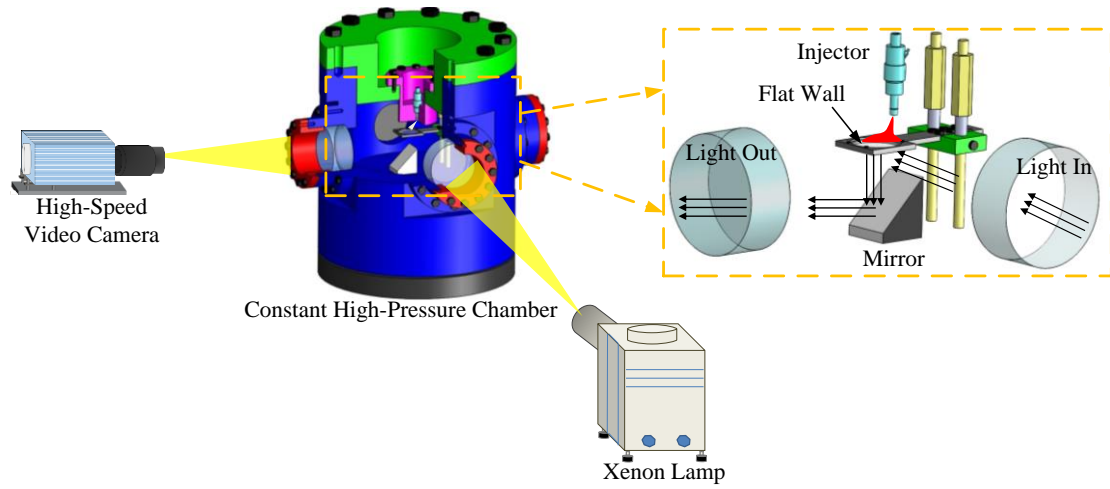
Figure 2. Experimental apparatus of RIM for fuel adhesion measurement
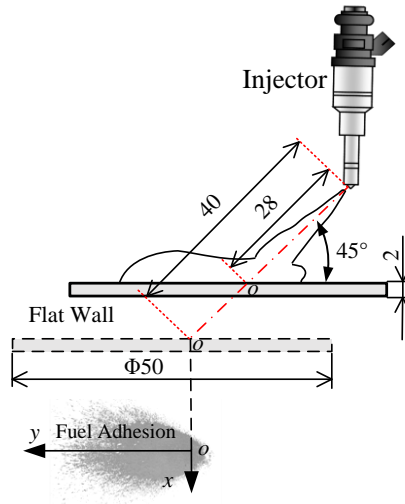
Figure 3. Schematic of injector and flat wall (All lengths are in millimeters)

Front View (Mie scattering)

Side View (Mie scattering)

Bottom View (RIM)
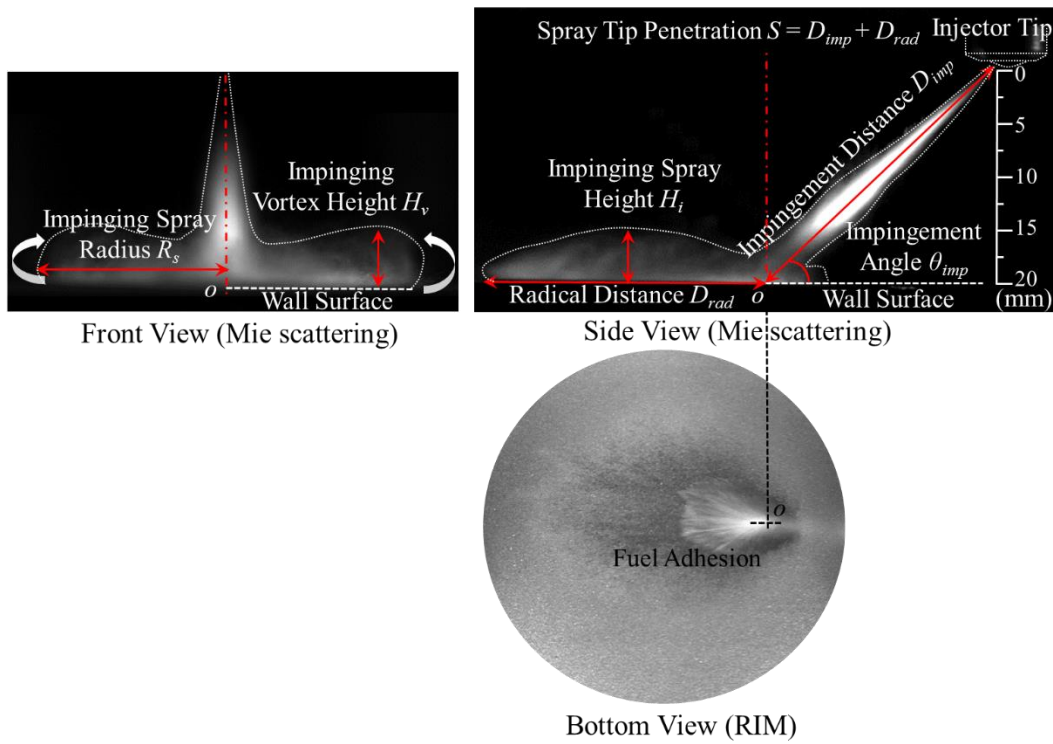
Figure 4. Definitions from three views of the impinging spray
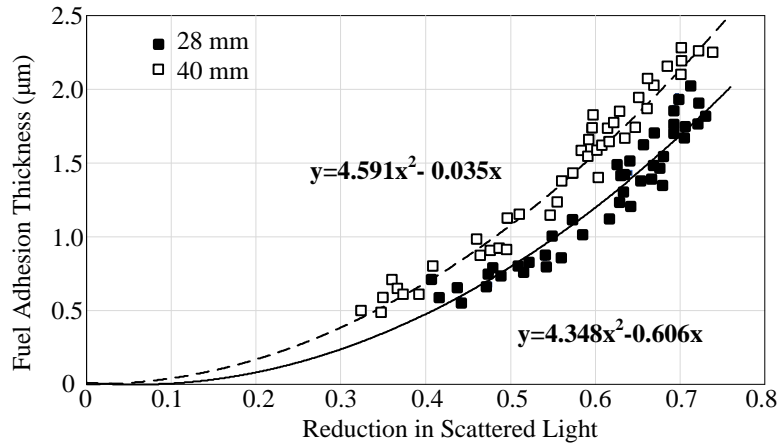
Figure 5. Calibration curves of different impingement distances

The two fitted curves are labeled:

$$y = 4.591x^2 - 0.035x$$

$$y = 4.348x^2 - 0.606x$$

(a)Dry Image   (b) Wet Image   (c)Background Removed Image   (d)Thickness Distribution Image
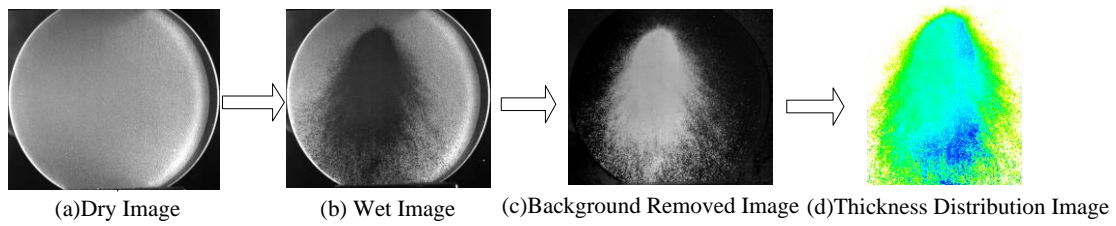
Figure 6. Image processing

(a) P_{inj} = 10 MPa   (b) P_{inj} = 20 MPa   (c) P_{inj} = 30 MPa
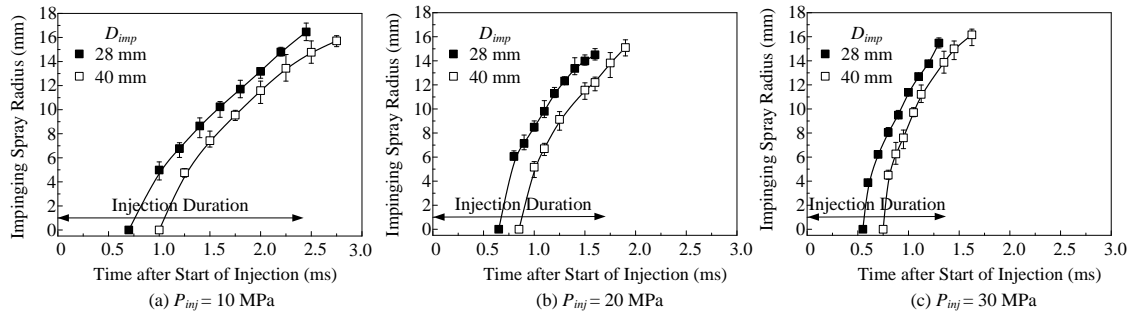
Figure 7. Impinging spray radius, R_s (Front view)

(a) P_{inj} = 10 MPa   (b) P_{inj} = 20 MPa   (c) P_{inj} = 30 MPa
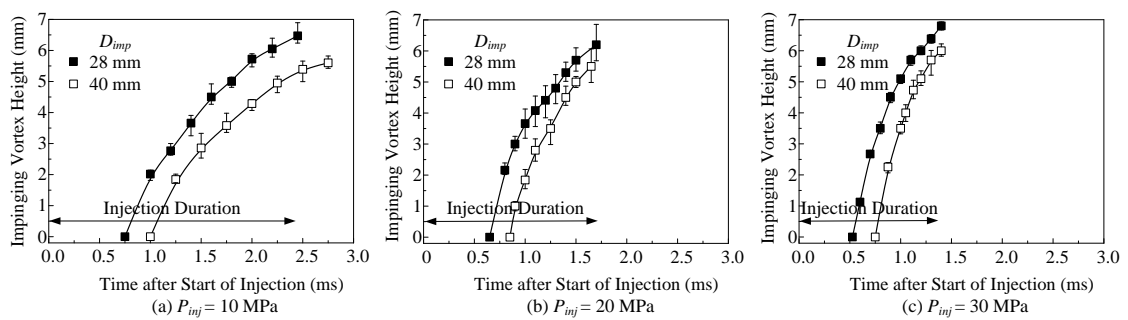
Figure 8. Impinging vortex height, H_v (Front view)
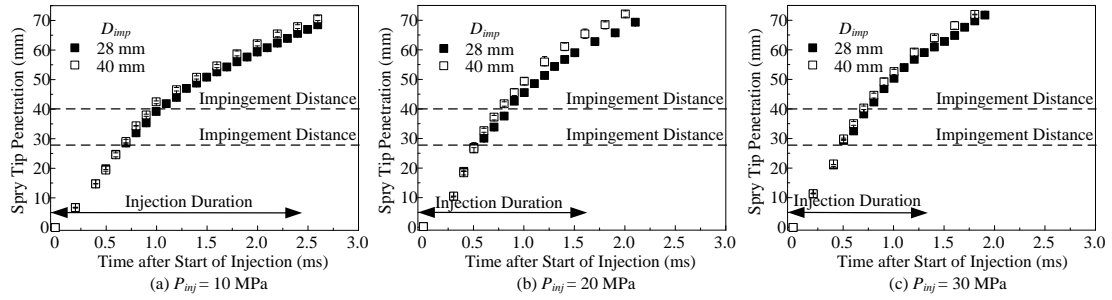
Figure 9. Spray tip penetration, S (Side view)
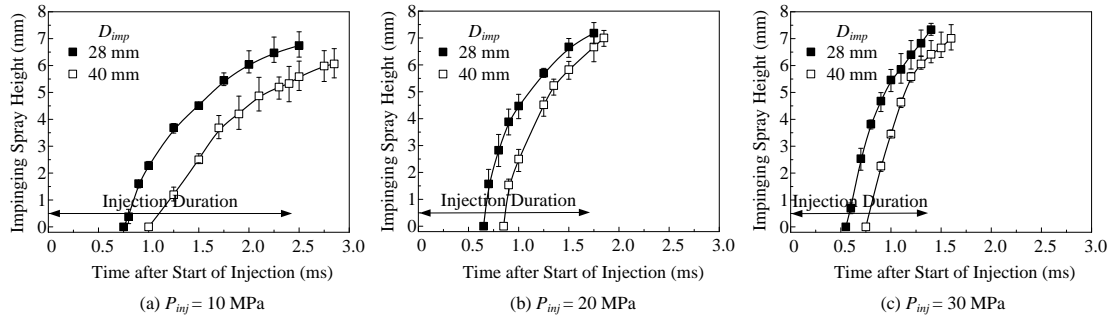
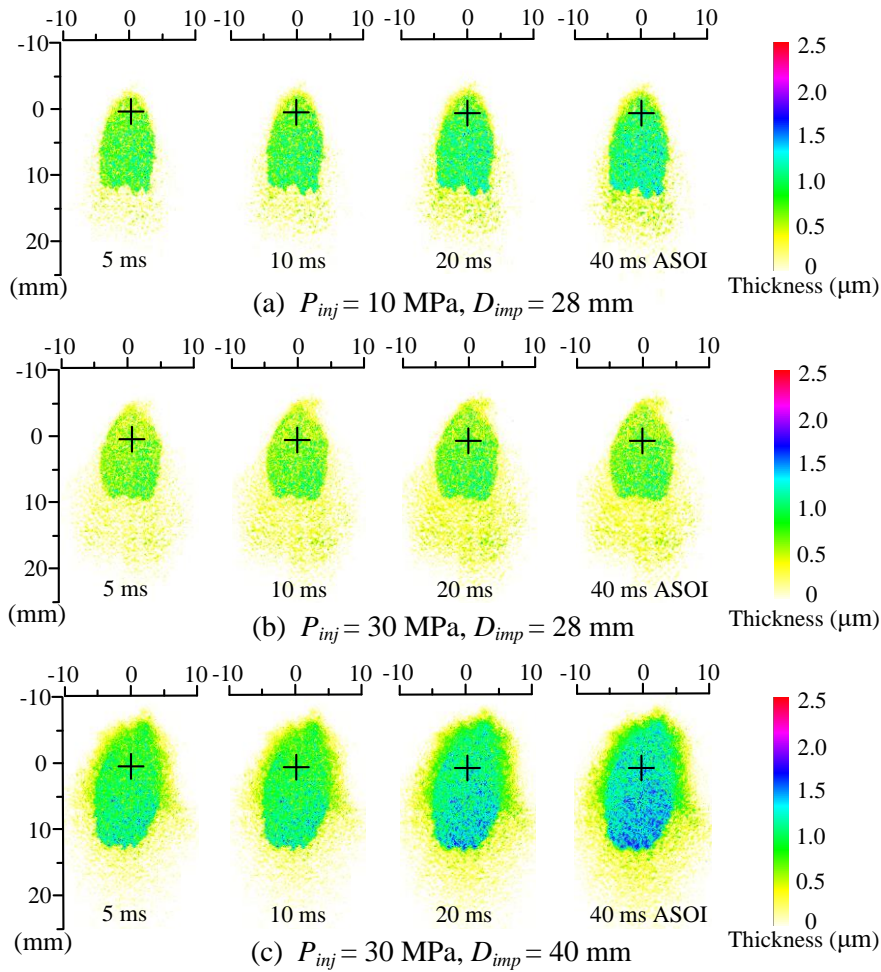**Figure 10.** Impinging spray height, H_i (Side view)
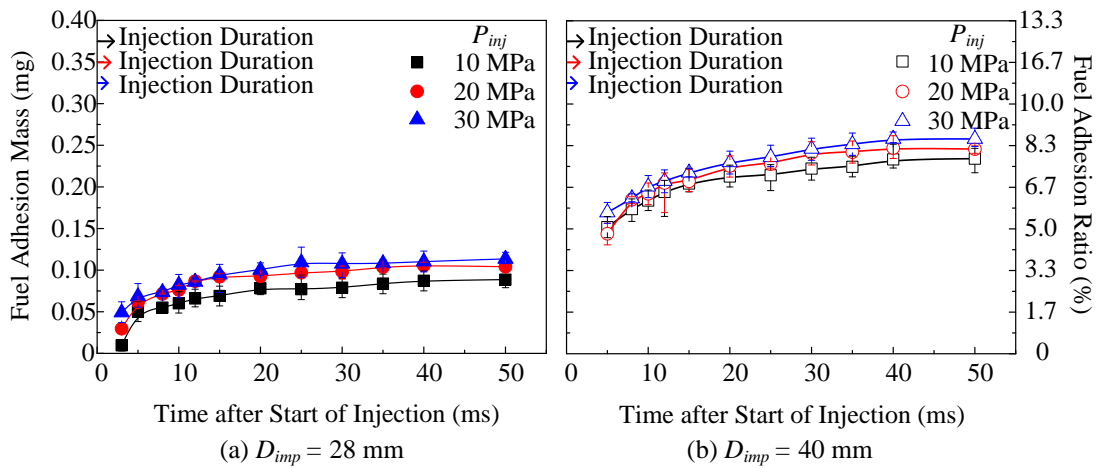

Figure 11. Fuel adhesion evolution (Bottom view)

(a) $D_{imp} = 28$ mm

(b) $D_{imp} = 40$ mm

Figure 12. Fuel adhesion mass

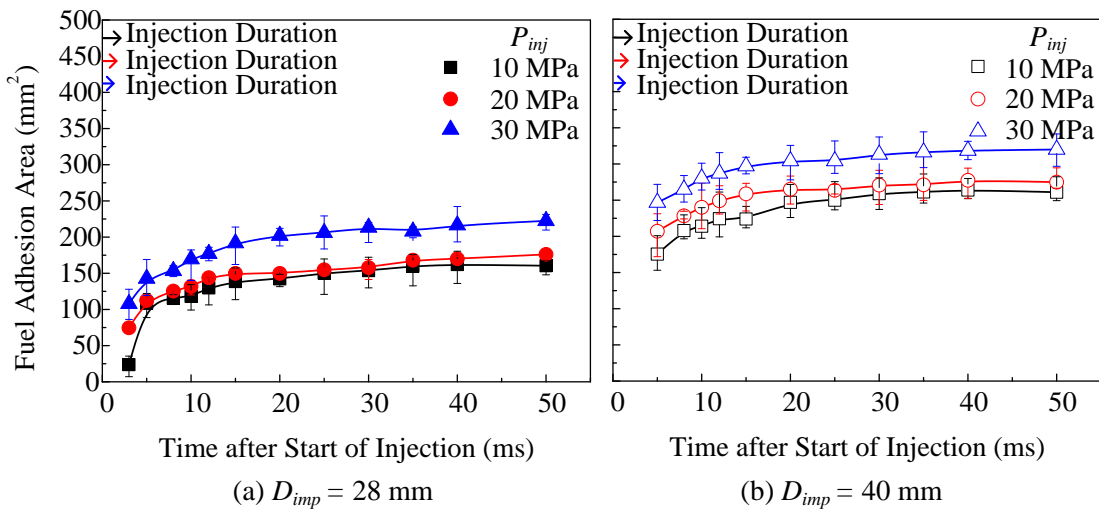(a) $D_{imp} = 28$ mm
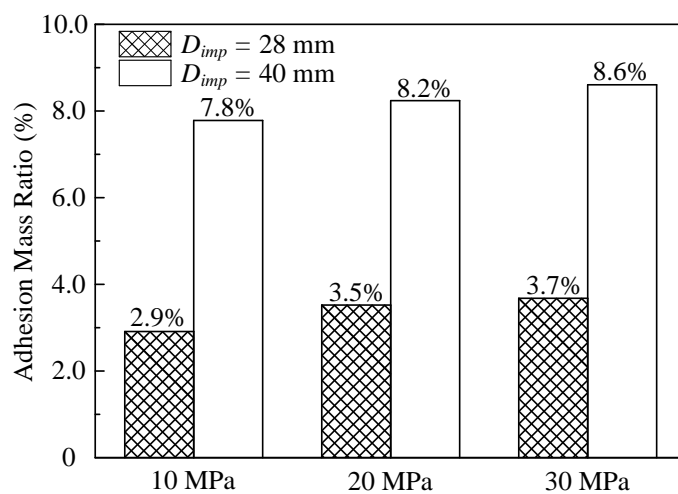
(b) $D_{imp} = 40$ mm

Figure 13. Fuel adhesion area

Figure 14. Adhesion mass ratio (40 ms ASOI)
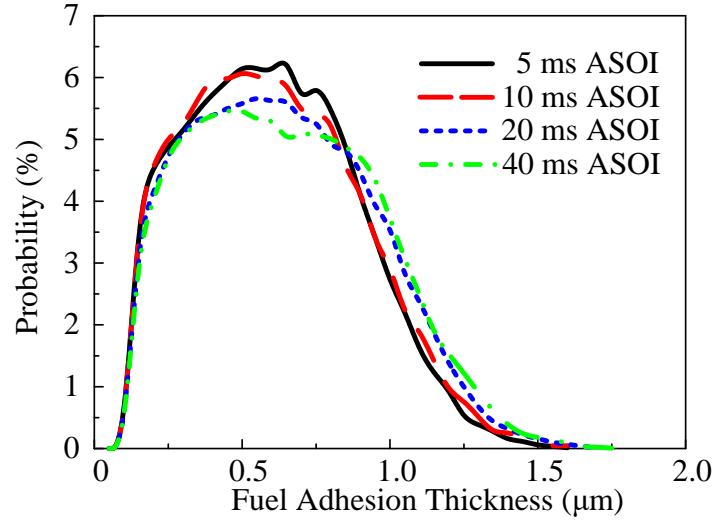
Figure 15. Probability of thickness with time (P_{inj} = 30 MPa, D_{imp} = 28 mm)
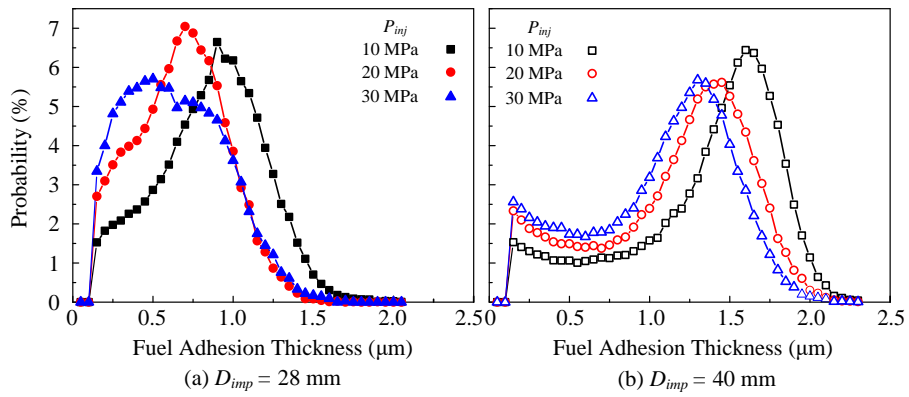

(a) D_{imp} = 28 mm

(b) D_{imp} = 40 mm

Figure 16. Probability of fuel adhesion thickness (40 ms ASOI)
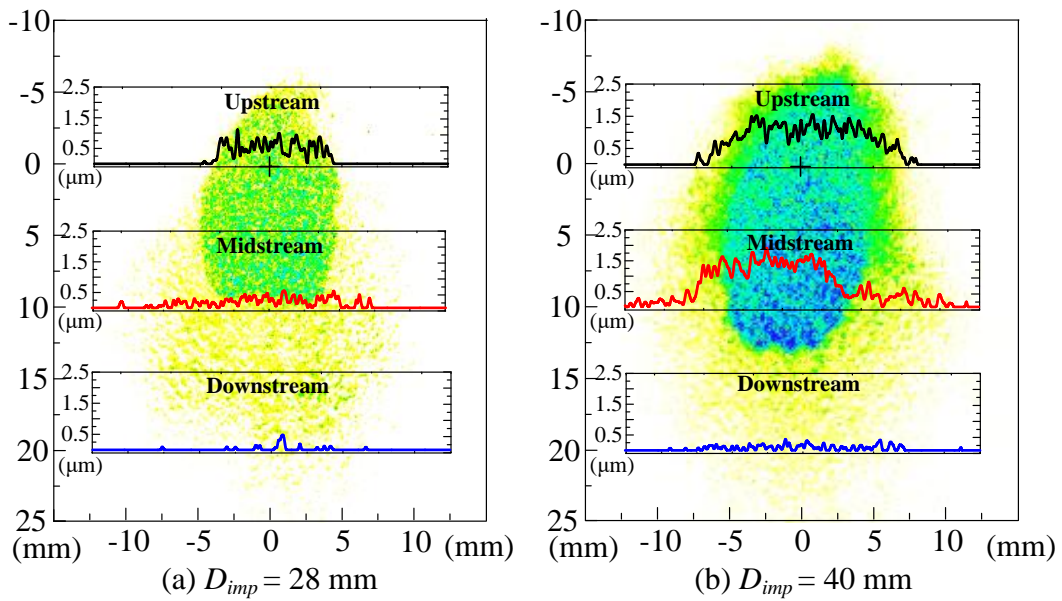

(a) D_{imp} = 28 mm

(b) D_{imp} = 40 mm

Figure 17. Fuel adhesion thickness distribution (40 ms ASOI)

Tables:

Table 1. Experimental conditions

Injection Conditions	
Fuel	Toluene
Injection Mass (M_{inj})	3.0 mg
Injection Pressure (P_{inj})	10, 20, 30 MPa
Injector Type	Mini-Sac, Single-Hole
Nozzle Hole Diameter (d)	0.135 mm
Injection Duration (t_d)	2.4, 1.65, 1.36 ms
Ambient Conditions	
Ambient Gas	Nitrogen
Pressure (P_{amb})	0.5 MPa
Temperature (T_{amb})	300 K
Density (ρ_{amb})	5.95 kg/m³
Impingement Conditions	
Impingement Plate	Quartz Glass
Impingement Distance (D_{imp})	28, 40 mm
Impingement Angle (θ_{imp})	45°
Surface Roughness	Ra7.5

Table 2. Characteristics of fuels and quartz glass

Parameter	Refractive Index	Density (kg/m³)	Boiling Point (K)	Kinematic Viscosity (10^{-6} m²/s)	Surface Tension (N/m)
Toluene	1.49	866	382.75	0.68	0.0285
Tridecane	1.43	756	507.58	2.35	0.0303
Gasoline	1.42	737	-	0.46	0.022
Quartz Glass	1.46	-	-	-	-